iScience

CellPress
OPEN ACCESS

Article

Demethylase FTO-mediated m6A modification of SIK1 modulates placental cytotrophoblast syncytialization in type 2 diabetes mellitus

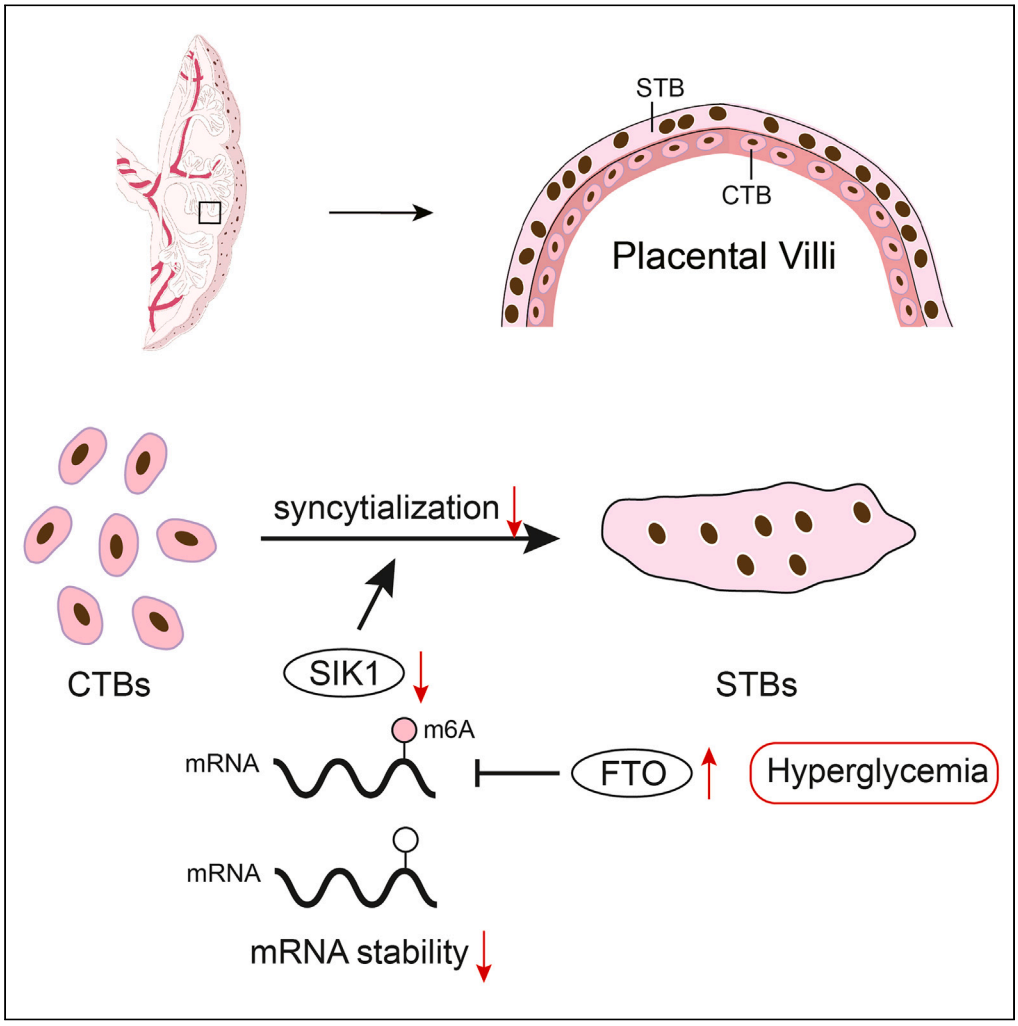

Jie Ning, Jie Yan, Shuxian Wang, Zifeng Cui, Yiwei Xue, Juan Juan, Huixia Yang

yanghuixia@bjmu.edu.cn

Highlights

Impaired syncytialization function occurs in hyperglycemia

m6A RNA methylation pattern is altered in trophoblasts exposed to hyperglycemia

FTO-mediated m6A modification of SIK1 modulates cytotrophoblast syncytialization

Ning et al., iScience *27*, 109900
June 21, 2024
https://doi.org/10.1016/j.isci.2024.109900

iScience

CellPress
OPEN ACCESS

Article

Demethylase FTO-mediated m6A modification of SIK1 modulates placental cytotrophoblast syncytialization in type 2 diabetes mellitus

Jie Ning,[1,2,3,4] Jie Yan,[1,2,4] Shuxian Wang,[1,2,3] Zifeng Cui,[1,2,3] Yiwei Xue,[1,2,3] Juan Juan,[1,2] and Huixia Yang[1,2,3,5,*]

SUMMARY

Type 2 diabetes mellitus (T2DM) represents a common complication during pregnancy that affects feto-placental development. We demonstrated the existence of impaired trophoblast syncytialization under hyperglycemic conditions. However, the exact mechanism remains unknown. RNA N6-methyladenosine (m6A) is an emerging regulatory mechanism of mRNA and participates in various biological processes. We described the global m6A modification pattern in T2DM placenta by the combined analysis of methylated RNA immunoprecipitation sequencing (MeRIP-Seq) and RNA sequencing (RNA-Seq). Both the m6A modification and expression of *SIK1*, which is critical for syncytialization, were significantly decreased in trophoblast exposed to hyperglycemic conditions. In addition, the m6A demethylase fat mass and obesity-associated protein (FTO) affects the expression and mRNA stability of *SIK1* by binding to its 3′-untranslated region (UTR) m6A site. This work reveals that the FTO-m6A-SIK1 axis plays critical roles in regulating syncytialization in the placenta.

INTRODUCTION

The placenta is a dynamic and complex organ essential for the maintenance of pregnancy and the development of the fetus. Mononucleated cytotrophoblast (CTB) fusion leading to the formation of a multinucleated syncytiotrophoblast (STB) layer or syncytium is a process referred to as syncytialization. Syncytialization is one of the hallmarks of placental development, ensuring placental hormone synthesis and nutrient exchange between the maternal and fetal circulation and constituting a biophysical barrier against infections.[1,2] Approximately two weeks after conception, syncytialization starts and subsequently continues until the end of pregnancy.[1,3] Trophoblast fusion is associated with the downregulation of E-cadherin and the upregulation of human chorionic gonadotropin (hCG) and syncytin-2 (SYNC-2).[1] Although this biological process is highly regulated, aberrations in syncytialization may have deleterious effects on pregnancy support.

Pregestational diabetes mellitus (PGDM), which includes the occurrence of either type 1 diabetes mellitus (T1DM) or type 2 diabetes mellitus (T2DM), creates an unfavorable environment for embryonic and fetoplacental development.[4,5] Different durations, degrees, and timings in the onset of hyperglycemic conditions during pregnancy might lead to diverse outcomes, and earlier exposure, particularly during placentation and fetal organogenesis, has more severe and greater long-term consequences than later exposure. Due to its adverse effects on placentation, a severe hyperglycemic environment may lead to reduced placental size and intrauterine growth retardation, despite an excess supply of maternal nutrients.[6,7] Some evidence has suggested the effects of hyperglycemia on trophoblast proliferation, apoptosis and cell cycle control during pregnancy,[8] and SYNC-2 and its receptor have also been shown to be reduced in the hyperglycemia-exposed placenta.[9] However, the exact mechanism of the effect of hyperglycemia on syncytialization is not yet fully understood.

The regulation of the transcriptome is key to supporting diverse biological processes, and m6A methylation, one of the most prevalent epitranscriptomic modifications in eukaryotes, can modify RNAs dynamically and reversibly.[10] The installation of m6A on mRNAs is catalyzed by the RNA methyltransferase complex, which is mainly composed of methyltransferase-like 3 (METTL3), METTL14, Wilms' tumor 1-associated protein (WTAP) and RNA-binding motif protein 15 (RBM15) are known as writers. Demethylation is mediated by the erasers (fat-mass and obesity-associated protein (FTO) and alkylation repair homolog protein 5 (ALKBH5)).[11] In addition, m6A is recognized by m6A-binding proteins, such as the YT521-B homology (YTH) domain family (YTHDF1/2/3), YTH domain containing (YTHDC1/2), and heterogeneous nuclear ribonucleoprotein A2B1 (HNRNPA2B1), also known as readers.[12] Recently, the effects of m6A modification on some common diseases during pregnancy have been reported, including preeclampsia,[13,14] spontaneous abortion,[15,16] gestational diabetes mellitus,[17] and obesity.[18,19]

[1]Department of Obstetrics and Gynecology and Reproductive Medicine, Peking University First Hospital, Beijing, China
[2]Beijing Key Laboratory of Maternal Fetal Medicine of Gestational Diabetes Mellitus, Beijing, China
[3]Peking University, Beijing, China
[4]These authors contributed equally
[5]Lead contact
*Correspondence: yanghuixia@bjmu.edu.cn
https://doi.org/10.1016/j.isci.2024.109900

Furthermore, a previous study found that the m6A level was decreased in the blood of patients with type 2 diabetes,[20] but the underlying molecular mechanisms involved in the modulation and biological function of m6A modification within the placenta of women with type 2 diabetes remain unknown.

Here, we aimed to identify gene-specific expression changes in m6A that may regulate placental gene expression by comparing placentas from women with type 2 diabetes to those from women with normal pregnancies. To this end, we used methylated RNA immunoprecipitation sequencing (MeRIP-seq) to explore its involvement in placental development and function. Furthermore, we also explored whether trophoblast syncytialization and its related gene expression were regulated by m6A modification during the forskolin (FSK)-induced fusion of BeWo cells to validate the underlying mechanism of abnormal placental development in type 2 diabetes.

RESULTS

Impaired syncytialization due to hyperglycemic exposure

We measured trophoblast syncytialization in the placenta of women with type 2 diabetes. We found that the immunohistochemical signals for β-hCG and SYNC-2 were mainly in STBs, and the signal intensity was stronger in the CTRL placenta ($p < 0.001$, Figure 1A, B). Then, we also evaluated syncytialization using the FSK-induced *in vitro* trophoblast fusion model exposed to hyperglycemia. We found that following the duration of FSK treatment, the mRNA expression of β-hCG and SYNC-2 increased gradually along with the induction time, and it was decreased in BeWo cells exposed to hyperglycemia between 48 h and 96 h ($p < 0.05$, Figure 1C). We also found that after 48 h of FSK treatment, the protein levels of β-hCG and SYNC-2 were decreased with 25 mmol/L glucose compared with 5.5 mmol/L glucose (Figure 1D). In addition, in BeWo cells treated with DMSO (FSK (−)), E-cadherin staining was detected mainly around individual cells. However, when treated with 20 μM FSK, BeWo cells gradually lost E-cadherin staining and became multinucleated, which indicated that cell fusion had occurred. Our results suggested that in BeWo cells treated with 25 mM glucose, the fusion index was lower than that of cells treated with 5.5 mM glucose ($p < 0.05$, Figure 1E). These results support the occurrence of impaired syncytialization function in hyperglycemia.

m6A RNA methylation is altered in trophoblasts exposed to hyperglycemia

m6A levels in total RNA were significantly lower in placenta samples of women with type 2 diabetes than in the CTRL group ($p < 0.05$, Figure 2A). Treatment with 25 mM glucose induced a significant decrease in m6A methylation compared to 5.5 mM glucose treatment in BeWo cells ($p < 0.001$, Figure 2B). These results suggest that m6A levels are sensitive to hyperglycemia, which may be related to trophoblast dysfunction during type 2 diabetes.

Then, we performed MeRIP-seq and RNA-seq in selected placentas ($n = 5$) of the two groups. In this experiment, each sample produced approximately 40 M MeRIP-seq, with 6962 m6A special peaks occurring in the T2DM group and 6984 special peaks in the CTRL group (Figure 2C). Each gene may have one or more modified peaks. The identified m6A peaks were mainly concentrated near the stop codon and the 3′-UTRs (Figure 2D, E). Additionally, the m6A peaks were both characterized by the GKACU (K = G/U) motif (Figure 2F). All significantly differentially methylated sites (fold change ≥2 or <0.5, and $p < 0.00001$) between the two groups are shown in Data S1.

GO analysis revealed that the abnormally regulated peaks in the T2DM group were significantly involved in the regulation of signal transduction, developmental processes, and transmembrane transport (Figures S1A and S1B). Kyoto Encyclopedia of Genes and Genomes (KEGG) pathway analysis suggested that the upregulated peaks in the T2DM group were significantly associated with the MAPK signaling pathway, calcium signaling pathway, PI3K-Akt signaling pathway, and others. The downregulated peaks were significantly associated with the synaptic vesicle cycle, insulin resistance, glucagon signaling pathway, and others (Figure 2G).

The m6A modification of SIK1, which is related to syncytialization, is significantly decreased in the placenta of women with type 2 diabetes

We focused on the genes with altered methylated m6A peaks that were related to placental development and trophoblast function, and these genes are listed in Table 1. To explore the targets of m6A modification that exert pivotal functions in the placenta of women with type 2 diabetes, we performed a combined analysis of MeRIPseq and RNA-seq data. Then, the significantly differentially expressed genes (fold change ≥2 or <0.5, and $p < 0.05$) between the two groups were identified using a volcano plot (Figure 3A), and these included 236 upregulated genes and 235 downregulated genes (Data S2). Based on the combined analysis, genes with significant differences in m6A levels and gene expression were divided into four groups which included 15 hypermethylated m6A peaks in mRNA transcripts that were significantly upregulated (11; hyper-up) or downregulated (4; hyper-down) and 28 hypomethylated m6A peaks in mRNA transcripts that were significantly upregulated (4; hypo-up) or downregulated (24; hypo-down) (Figure 3B, Data S3). The data visualization analysis of specific modifications is shown in Figure 3C.

Based on gene function, we ultimately selected SIK1,[21] ADAMDEC1,[22] TET1[23] and AR,[24] which are related to syncytialization. The enriched KEGG pathways of the MAPK and PI3K-Akt signaling pathways were also involved in syncytialization.[25] To verify the sequencing analysis, we demonstrated that m6A levels of SIK1-site ($p < 0.01$) and ADAMDEC1-site ($p < 0.0001$) were significantly downregulated in the T2DM group, and TET1-site ($p < 0.01$), AR-site1 ($p < 0.01$), and AR-site2 ($p < 0.0001$) were significantly upregulated in T2DM group (Figure 4A), which was consistent with the results of MeRIP-Seq. In addition, we verified the different m6A-methylation statuses of ASCL2, DIO2, FGFR2, HGF and MYC, which are also involved in placental development (Figures S2A-S2E).[26–29] The mRNA levels of SIK1, ADAMDEC1, and TET1 were significantly lower and the mRNA level of AR was significantly higher in BeWo cells treated with 25 mM glucose, and the mRNA levels of SIK1 and AR

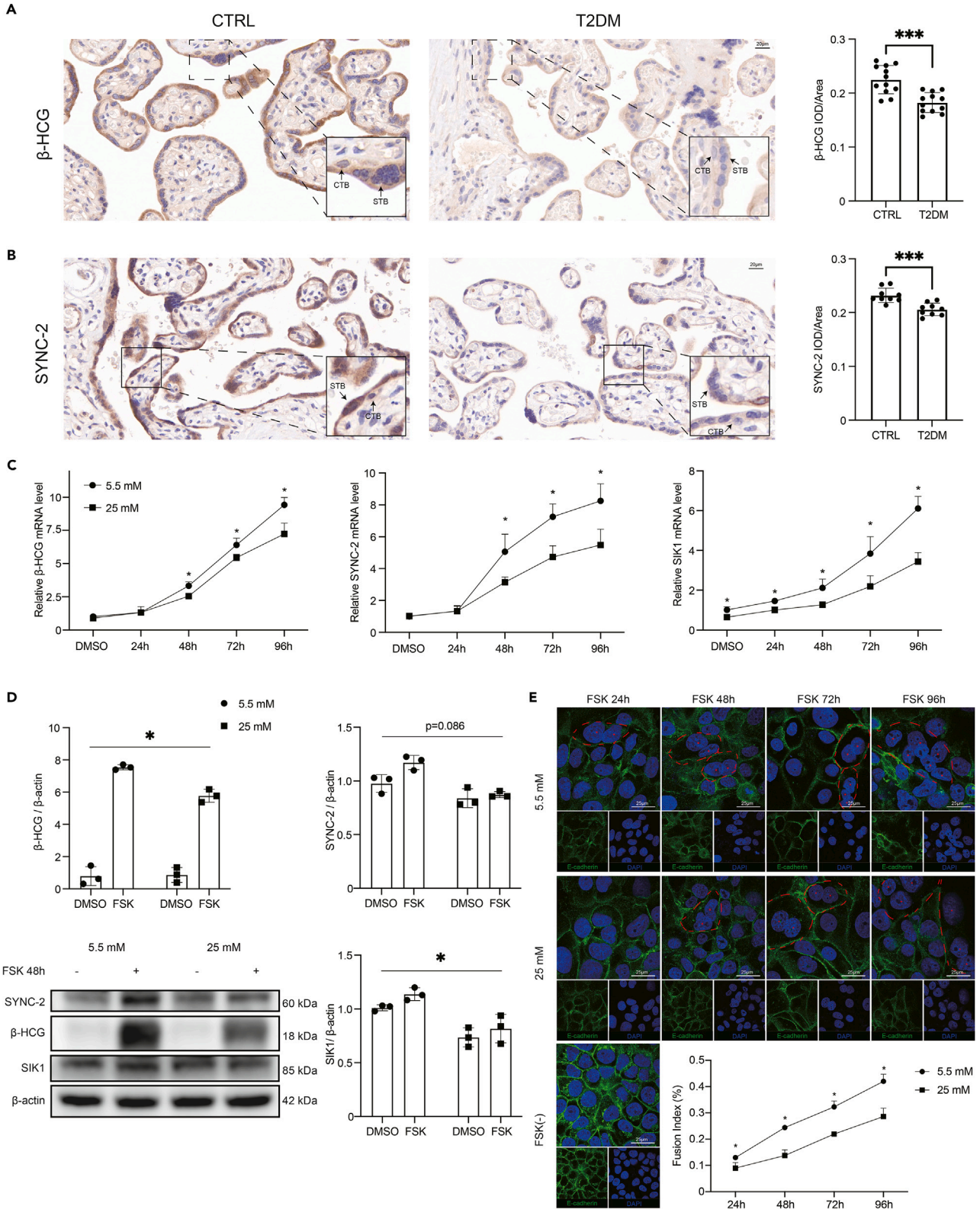
A
CTRL
T2DM
β-HCG
CTB
STB
β-HCG IOD/Area
***
CTRL
T2DM
B
SYNC-2
SYNC-2 IOD/Area
C
5.5 mM
25 mM
Relative β-HCG mRNA level
Relative SYNC-2 mRNA level
Relative SIK1 mRNA level
DMSO
24h
48h
72h
96h
D
β-HCG / β-actin
SYNC-2 / β-actin
p=0.086
SIK1/ β-actin
DMSO FSK
FSK 48h
SYNC-2
β-HCG
SIK1
β-actin
60 kDa
18 kDa
85 kDa
42 kDa
E
FSK 24h
FSK 48h
FSK 72h
FSK 96h
FSK(-)
E-cadherin
DAPI
Fusion Index (%)

Figure 1. Impaired syncytialization due to hyperglycemic exposure

(A) Immunohistochemical localization and expression of β-hCG in the placenta of the T2DM group and CTRL group at 400× magnification (Scale bar, 20 μm).

(B) Immunohistochemical localization and expression of SYNC-2 in the two groups at 400× magnification.

(C) BeWo cells were treated with 20 μM FSK for 24 h, 48 h, 72 h, and 96 h or DMSO at 5.5 mM or 25 mM glucose, and the mRNA expression of β-hCG, SYNC-2, and SIK1 was analyzed by real-time quantitative polymerase chain reaction (RT−qPCR).

(D) Western blotting (WB) detection of the protein expression of β-hCG, SYNC-2, and SIK1 in BeWo cells treated with 20 μM FSK for 48 h or DMSO at 5.5 mM or 25 mM glucose.

(E) E-cadherin was examined by immunofluorescence (green) and nuclei were stained with DAPI (blue). The multinucleated cells are shown in the red dotted frame and their nuclei are marked with red asterisks (Scale bar, 25 μm). Cell fusion at 24 h, 48 h, 72 h, and 96 h was evaluated and quantified via the fusion index, as described in the STAR Methods. Results were analyzed using unpaired t-test (for parametric data) or the Mann–Whitney test (for nonparametric data) and data are represented as mean ± SD. *$p < 0.05$, ***$p < 0.001$. T2DM: Type 2 diabetes mellitus in pregnancy; CTRL: healthy control; CTB: cytotrophoblast; STB: syncytiotrophoblast; IOD: integrated optical density; FSK: forskolin; DMSO: dimethyl sulfoxide.

in the placenta of women with type 2 diabetes showed the same trend (Figure 4B, C). Considering the low expression of AR in the term placenta and the combined analysis, our subsequent experiments mainly focused on SIK1. The expression of SIK1 protein in the placenta of women with type 2 diabetes was significantly lower, and the same trend was also shown in BeWo cells treated with 25 mM glucose (Figure 4D, E). Additionally, we found that hyperglycemia affected the stability of SIK1 mRNA ($p < 0.05$, Figure 4F). In FSK-induced BeWo cells, the expression of SIK1 was also decreased when exposed to hyperglycemia ($p < 0.05$, Figure 1C, D). Moreover, to validate the importance of the SIK1 gene in BeWo fusion, we used siRNA to knockdown SIK1 in BeWo cells. Our results showed that the FSK-induced upregulation of β-hCG and SYNC-2 expression was reduced in SIK1-knockdown cells (SIK1 si) (Figure 4G, H). In addition, our results showed that cell fusion was blocked in SIK1 si BeWo cells after FSK treatment (Figure 4I).

Hyperglycemia-associated upregulation of the demethylase FTO suppresses SIK1 expression and cell fusion

The hyperglycemia-related decrease in global and SIK1 mRNA m6A methylation could be mediated by the imbalance of m6A writers and erasers. Previously, we have demonstrated that hyperglycemia could upregulate the expression and nuclear translocation of METTL3 in trophoblasts.[30] In this study, our results showed that the expression and nuclear location of FTO ($p < 0.05$) were significantly upregulated in trophoblasts from the placenta of women with type 2 diabetes (Figure 5A). No statistically significant differences were observed in the mRNA levels of other m6A modification-related proteins in the placentas of the two groups ($p > 0.05$, Figure S3A). In the group of BeWo cells treated with 25 mM glucose, we observed that the expression of FTO was significantly increased (Figure 5B). The mRNA levels of METTL14 and ALKBH5 were also significantly increased in BeWo cells treated with 25 mM glucose, while the mRNA level of WTAP was significantly decreased (Figure S3B).

Next, we examined the regulatory effect of FTO on SIK1 and observed a significant decrease in the mRNA and protein expression of SIK1, as well as a decrease in the stability of SIK1 mRNA, upon the overexpression of FTO (Figures 5C and 5D). In addition, the suppression of SIK1 expression during exposure to hyperglycemia (25 mM glucose) was rescued by transfection with FTO-siRNA (Figure 5E). Through the dual-luciferase reporter assay, we found that FTO regulated the expression of SIK1 via recognition of SIK1 mRNA m6A motifs in the 3′-UTR. Compared to the co-transfection MUT group, the relative luciferase activity was lower in the FTO-DN plasmid and WT-SIK1 cotransfection group ($p < 0.05$, Figure 5F), indicating that there was a direct interaction between FTO and SIK1. These results indicated that hyperglycemia regulates SIK1 expression in BeWo cells, which is related at least in part to the upregulation of FTO.

To further explore the role of FTO in trophoblast syncytialization, we next treated BeWo cells transfected with negative control (CTRL) or FTO-DN plasmid (FTO OE) with 20 μM FSK for 48 h. Figure 5G indicates that the FSK-induced mRNA upregulation of β-hCG and SYNC-2 was reduced in FTO OE BeWo cells compared with CTRL cells. The protein expression showed consistent changes (Figure 5H). The fusion index, which was reflected by E-cadherin staining, was also decreased in FTO OE BeWo cells ($p < 0.05$, Figure 5I). The upregulated expression of SIK1 induced by FSK treatment was also inhibited by FTO overexpression (Figure 5G, H). Our results indicated that FTO overexpression could repress FSK-induced cell fusion in BeWo cells.

DISCUSSION

The present study indicated that there was a potential mechanism of impaired syncytialization associated with m6A methylation in placental tissue samples from type 2 diabetes patients. The mRNA stability and expression of SIK1, the key factor in syncytialization, was downregulated by elevated FTO in trophoblasts exposed to hyperglycemia via a m6A methylation-dependent mechanism, which may subsequently lead to impaired trophoblast fusion.

The trophoblast syncytialization process is associated with the enrichment of genes involved in the transport of amino acids, iron and glucose, and an impaired syncytialization process might be related to abnormal placental function.[31–33] Only a few studies have reported that SYNC-2 and its receptor were decreased in placental tissue exposed to hyperglycemia.[9] Here, we provide evidence that severe hyperglycemia affects syncytialization by morphological and functional differentiation using an *in vitro* trophoblast fusion model. Both of the fusion index and the expression of the markers for syncytialization, β-hCG and SYNC-2, were decreased when exposed to hyperglycemia. Kuc S et al.[34] also proposed that while hyperglycemia is thought to trigger excessive fetal growth, impaired early placentation might be the reason for the normal birthweight instead of macrosomia in PGDM offspring. Defective syncytialization might lead to nutrient transfer imbalance, ultimately compromising fetal development.

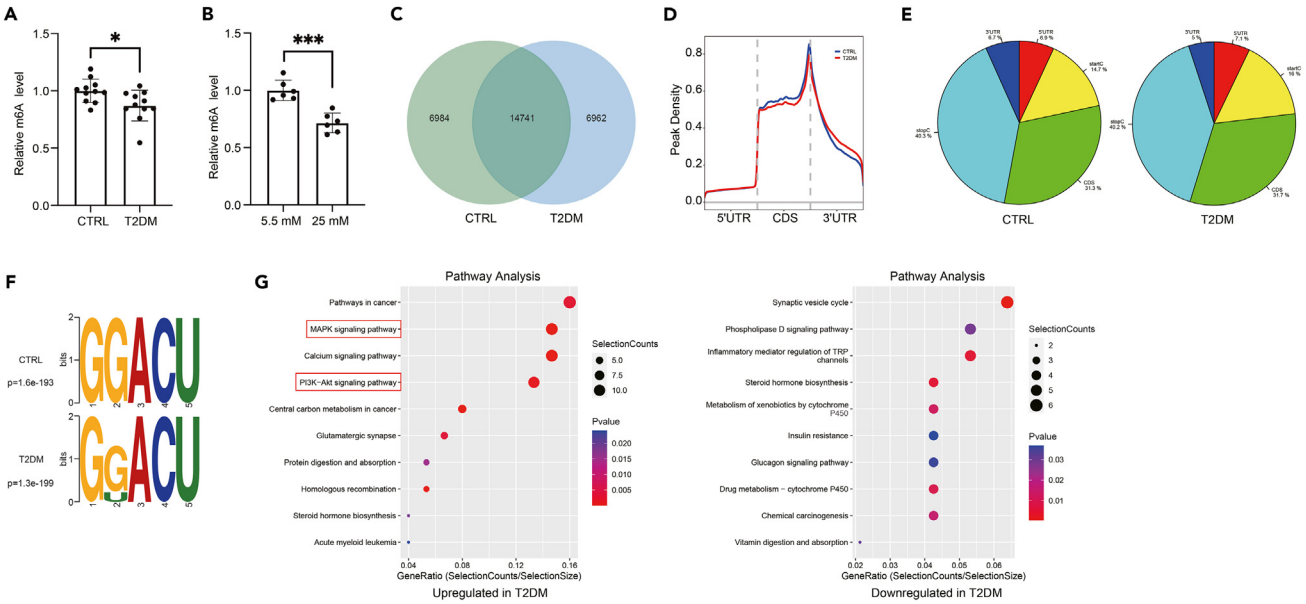

Figure 2. Overview of the m6A methylation landscape in placenta samples

(A, B) The EpiQuik M6A RNA Methylation Quantification Kit was used to detect m6A levels in the RNA samples from the placentas and BeWo cells.

(C) Venn diagram displaying the special and common m6A peaks in the T2DM and CTRL groups.

(D) Metagene plots displaying the region of average m6A peaks throughout the transcripts of the two groups.

(E) Pie charts showing the distribution of m6A peaks in the two groups.

(F) Sequence motifs of the m6A-containing peak regions.

(G) The significantly enriched T2DM-related signaling pathways for the altered m6A peak transcripts (left: up; right: down). The results were analyzed by unpaired *t* test, and $p < 0.05$ was considered significant. Quantitative data are expressed as the mean ± SD. $*p < 0.05$, $***p < 0.001$. MeRIP-seq: m6A RNA immunoprecipitation sequencing; T2DM: Type 2 diabetes mellitus in pregnancy; CTRL: healthy control; UTR: untranslated region; CDS: coding sequence.

To date, knowledge of the specific regulatory mechanism of dysfunction in syncytialization is limited. In the preeclampsia placenta, markedly enhanced cystathionine γ-lyase (CSE) O-GlcNAcylation increases H2S production, repressing trophoblast syncytialization by hampering AR dimerization.[24] In addition, deletion of RBM15 causes defects in the spongiotrophoblast and STB layers.[35] As the most common modification of mammalian mRNA, m6A methylation regulates many aspects of RNA-associated metabolism process, such as RNA transcription, splicing, degradation, and translation.[12] Although m6A modification has recently been reported to be associated with the proliferation, invasion, migration, and apoptosis of trophoblastic cells,[36] studies on the effect of m6A modification on syncytialization are lacking. We found that both the expression and m6A modification of SIK1 were significantly decreased in the placenta of women with type 2 diabetes. SIK1, a member of the salt-inducible kinase family, is a serine/threonine protein kinase that belongs to the adenosine monophosphate-activated protein kinase (AMPK) subfamily and has emerged as a key regulator of metabolism. Two important groups of substrates for SIKs are cyclic adenosine monophosphate (cAMP)-response-element binding protein (CREB)-regulated transcriptional coactivators and the class 2a histone deacetylases (HDACs).[37,38] A previous study indicated that SIK1 plays a role in trophoblast fusion[21] and that the cAMP/cREB signaling pathway is a key pathway during syncytialization of trophoblast cells.[25] We also verified that hallmarks of trophoblast syncytialization were disrupted in the absence of SIK1.

In this study, we further clarified that the altered expression of SIK1 was related to FTO-mediated m6A demethylation under hyperglycemic conditions and that the overexpression of FTO affected FSK-induced syncytialization in BeWo cells, which is potentially part of the putative mechanism by which hyperglycemia affects syncytialization. FTO belongs to the AlkB family of nonheme Fe(II)/α-ketoglutarate (α-KG)-dependent dioxygenases, which catalyze a wide range of biological oxidation reactions, including the demethylation of m6A.[39] Previous studies suggested that m6A was significantly decreased in T2DM patients (nonpregnant patients), and FTO was positively correlated with serum glucose.[20] FTO is highly expressed in the placenta and is closely correlated with fetal growth and development in different maternal nutritional states.[40–42] FTO is potentially involved in the cellular sensing of amino acids through the mTORC1 pathway, which might regulate fetal growth.[43] In addition, FTO expression was significantly downregulated in the trophoblasts of spontaneous abortion patients with aberrant m6A accumulation, which was correlated with oxidative stress.[15] In addition, we previously showed the upregulation of METTL3 in the placenta of women with type 2 diabetes and BeWo cells treated with 25 mM glucose.[30] Altogether, the hyperglycemia-related decrease in m6A methylation may be regulated not only by the increase in the expression and subcellular localization of FTO but also by the variations in other m6A-related proteins, which might be counterbalanced by the concomitant increased expression of METTL3. Our results thus elucidate the potential pathogenic role of m6A modification in type 2 diabetes that is associated with placental dysfunction.

In conclusion, we have described the m6A RNA methylation landscape of the placenta of women with type 2 diabetes, and our findings suggest that the m6A eraser FTO-mediated m6A modification of SIK1 modulates human CTB syncytialization, which might be involved in

Table 1. Differentially m6A-modified genes related to placental development and trophoblast function

		MeRIP-seq					RNA-seq		
Gene name	Chr	Peak start	Peak end	FC	RDR	*p*-value	FC	RDR	*p*-value
LHX6	chr9	124966221	124966420	20.00	up	7.27E-09	2.12	up	0.0643
MEF2C	chr5	88026027	88026051	0.07	down	1.14E-07	1.58	up*	0.00405
FPR2	chr19	52271630	52271785	0.09	down	2.36E-08	0.95	down	0.959
ATP6V0D2	chr8	86999581	86999629	0.09	down	1.28E-07	2.61	up	0.271
ADAMDEC1	chr8	24249881	24249893	0.11	down	1.93E-08	1.39	up	0.730
AR	chrX	66765441	66765680	7.04	up	2.19E-06	14.96	up*	0.000870
DIO2	chr14	80678481	80678521	0.20	down	2.03E-07	0.33	down	0.126
AR	chrX	66946561	66946960	4.42	up	2.49E-07	14.96	up*	0.000870
TRPV4	chr12	110234329	110234509	3.99	up	6.30E-06	1.02	up	0.918
TFEB	chr6	41703087	41703265	3.67	up	3.35E-08	1.02	up	0.938
ASCL2	chr11	2291821	2292160	0.29	down	3.03E-07	0.29	down	0.0627
TET1	chr10	70333641	70333880	3.39	up	4.28E-08	1.21	up	0.349
SIAH1	chr16	48419141	48419229	3.34	up	9.32E-06	1.01	up	0.960
F2RL1	chr5	76128801	76129420	0.34	down	6.27E-07	0.68	down	0.674
PRDM1	chr6	106553461	106553760	2.46	up	8.15E-07	1.17	up	0.771
CYP1B1	chr2	38297841	38298400	2.27	up	2.53E-06	2.38	up	0.173
SIK1	chr21	44836401	44836960	0.49	down	8.50E-07	0.47	down*	0.00171
HGF	chr7	81392061	81392312	2.03	up	6.04E-07	1.92	up	0.0624

MeRIP-seq: m6A RNA immunoprecipitation sequencing; Chr: Chromosome; FC: fold change; RDR: regulation. *$p < 0.05$ for RNA-seq.

hyperglycemia-associated impaired placental function. However, the exact correlations between m6A levels and glycemic status and more hyperglycemia-related precise regulatory mechanisms of m6A methylation-modified RNA affecting the biological behaviors of trophoblasts remain to be discovered.

Limitations of the study

We also acknowledge the limitations of this study. While the FSK-induced fusion of BeWo cells is a well-established trophoblast cell line for the study of syncytialization, it does not reflect all the features of villous CTBs and STBs. More *in vivo* and *in vitro* models, such as human trophoblast stem cells, primary human trophoblasts, and organoids, are needed to generalize this conclusion.[44,45]

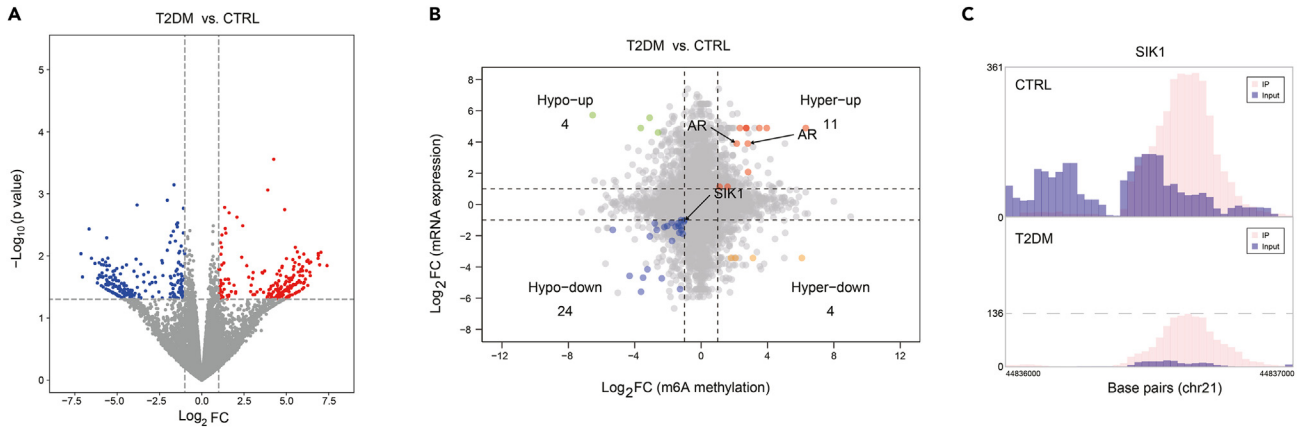

Figure 3. Conjoint analysis of MeRIP-seq and RNA-seq data

(A) Volcano plots displaying the mRNAs that were differentially expressed between the two groups (FC ≥ 2 or <0.5, and $p < 0.05$).

(B) Four-quadrant graph showing the distribution of transcripts with a significant change in both m6A level and mRNA expression in the T2DM group.

(C) Data visualization analysis of SIK1 mRNA m6A modifications in the T2DM and CTRL groups. MeRIP-seq: m6A RNA immunoprecipitation sequencing; T2DM: Type 2 diabetes mellitus in pregnancy; CTRL: healthy control; FC: fold change.

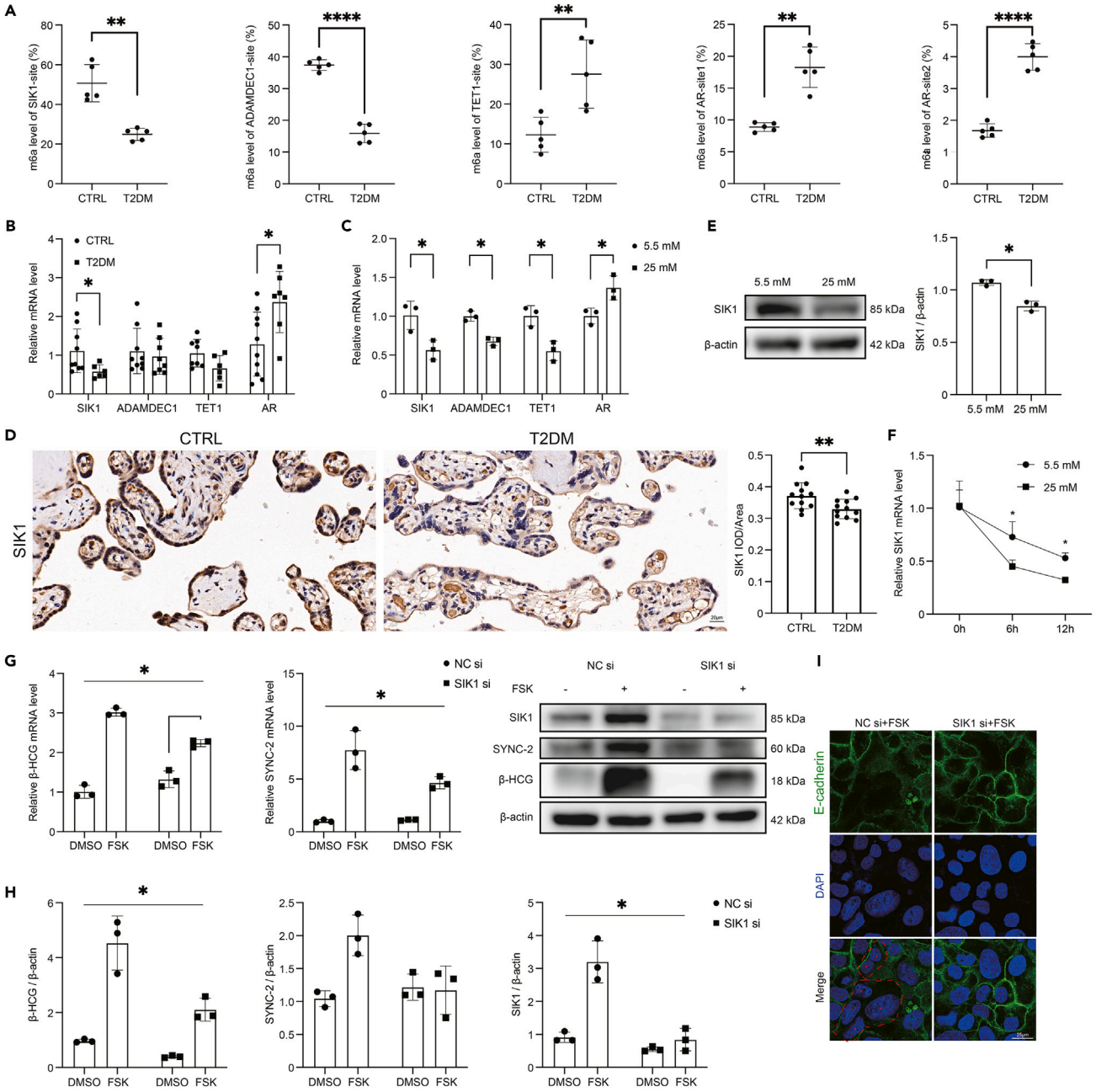

Figure 4. Verification of m6A methylation status, gene expression, and protein expression and the key role of SIK1 in syncytialization

(A) The m6A levels at specific sites of SIK1, ADAMDEC1, TET1 and AR.

(B) The mRNA levels of SIK1, ADAMDEC1, TET1 and AR in the placentas of the T2DM and CTRL groups.

(C) The mRNA expression of SIK1, ADAMDEC1, TET1 and AR in BeWo cells treated with 5.5 mM glucose or 25 mM glucose.

(D) Immunohistochemical localization and expression of SIK1 in the placentas of the T2DM and CTRL groups at 400× magnification (Scale bar, 20 μm).

(E) The protein expression of SIK1 in BeWo cells treated with 5.5 mM glucose or 25 mM glucose.

(F) The effect of hyperglycemia on the mRNA stability of SIK1 in BeWo cells.

(G) Control-siRNA BeWo cells (NC si) and SIK1-knockdown BeWo cells (SIK1 si) were treated with 20 μM FSK or DMSO for 48 h, and the mRNA expression of β-hCG and SYNC-2 was analyzed by real-time quantitative polymerase chain reaction (RT–qPCR).

(H) The protein expression of β-hCG, SYNC-2 and SIK1 was analyzed by Western blotting (WB) in above-mentioned BeWo cells.

(I) E-cadherin was examined by immunofluorescence (green), and nuclei were stained with DAPI (blue). The multinucleated cells are shown in the red dotted frame and their nuclei are marked with red asterisks (Scale bar, 25 μm). Results were analyzed using unpaired t-test (for parametric data) or the Mann–Whitney test (for nonparametric data) and data are represented as mean ± SD. *$p < 0.05$, **$p < 0.01$, ****$p < 0.0001$. T2DM: Type 2 diabetes mellitus in pregnancy; CTRL: healthy control; IOD: integrated optical density; FSK: forskolin; DMSO: dimethyl sulfoxide.

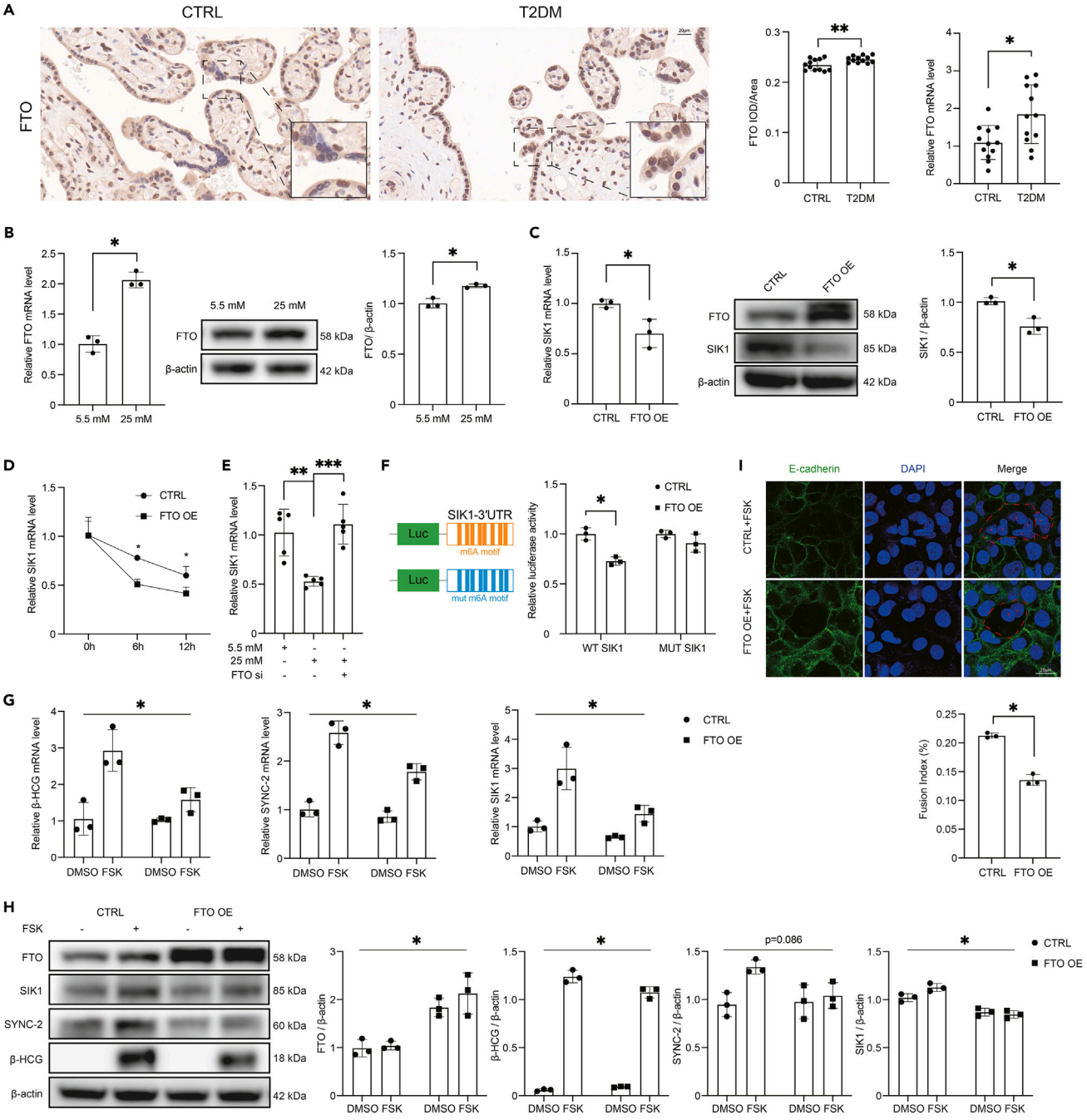

Figure 5. The expression of FTO and its regulatory effects on SIK1 and cell fusion

(A) Immunohistochemical localization and expression at 400× magnification and mRNA levels of FTO (Scale bar, 20 μm).

(B) mRNA expression and protein expression of FTO were quantified in BeWo cells by real-time quantitative polymerase chain reaction (RT–qPCR) and Western blotting (WB), respectively, after 48 h of 5.5 or 25 mM glucose treatment.

(C) The mRNA and protein expression levels of SIK1 in BeWo cells overexpressing FTO.

(D) The effect of FTO overexpression on the mRNA stability of SIK1 in BeWo cells.

(E) Effect of FTO inhibition on the mRNA expression of SIK1 in BeWo cells after 48 h of 25 mM glucose treatment.

(F) Relative luciferase activity of luciferase vectors with WT or MUT (A-to-T mutation) m6A sites in the SIK1 gene after cotransfection with negative (CTRL) or FTO-DN plasmid (FTO OE) into BeWo cells. Firefly luciferase activity was measured and normalized to Renilla luciferase activity.

(G and H) BeWo cells transfected with negative (CTRL) or FTO-DN plasmid (FTO OE) were treated with 20 μM FSK or DMSO for 48 h, and the mRNA levels (G) and protein levels (H) of β-hCG, SYNC-2, and SIK1 were analyzed by real-time quantitative polymerase chain reaction (RT–qPCR) and Western blotting (WB), respectively.

Figure 5. *Continued*

(I) E-cadherin was examined by immunofluorescence (green), and nuclei were stained with DAPI (blue). The multinucleated cells are shown in the red dotted frame and their nuclei are marked with red asterisks (Scale bar, 25 μm). The fusion index was used to evaluate and quantify cell fusion in FSK-induced BeWo cells transfected with negative control (CTRL) or FTO-DN plasmid (FTO OE). Results were analyzed using unpaired t-test (for parametric data) or the Mann–Whitney test (for nonparametric data) and data are represented as mean ± SD. *$p < 0.05$, **$p < 0.01$, ***$p < 0.001$. T2DM: Type 2 diabetes mellitus in pregnancy; CTRL: healthy control; IOD: integrated optical density; OE: overexpression; FSK: forskolin; DMSO: dimethyl sulfoxide.

STAR★METHODS

Detailed methods are provided in the online version of this paper and include the following:

- KEY RESOURCES TABLE
- RESOURCE AVAILABILITY
  - Lead contact
  - Materials availability
  - Data and code availability
- EXPERIMENTAL MODEL AND STUDY PARTICIPANT DETAILS
  - Human participants
  - Cell lines
- METHOD DETAILS
  - RNA m6A quantification
  - RNA extraction and real-time quantitative PCR (RT–qPCR)
  - Western blotting (WB)
  - Immunohistochemistry
  - MeRIP-seq and data analysis
  - RNA sequencing
  - Gene-specific m6A qPCR (MeRIP-qPCR)
  - Cell transfection
  - mRNA stability
  - Immunofluorescence and image analysis
  - Dual-luciferase reporter assays
- QUANTIFICATION AND STATISTICAL ANALYSIS

SUPPLEMENTAL INFORMATION

Supplemental information can be found online at https://doi.org/10.1016/j.isci.2024.109900.

ACKNOWLEDGMENTS

This work was supported by the National Key Research and Development Program of China (No. 2021YFC2700700 and No. 2021YFC2700702), the National Natural Science Foundation of China (No. 82371688 and No. 81830044), and National High Level Hospital Clinical Research Funding (No. 22cz020401-4811009).

AUTHOR CONTRIBUTIONS

J.N. performed and analyzed all the experiments and co-wrote the manuscript. J.Y. participated in the experimental design and helped to perform the experiments and co-wrote the manuscript. S.W. participated in sample collection and cell experiments. Z.C. participated in the data analysis and helped to modify the manuscript. Y.X. helped to perform the experiments. J.J. helped with the statistical analysis. H.Y. acquired funding and conceptualized, designed, supervised and interpreted all studies, co-wrote the manuscript and was the lead contact for this work. All authors contributed to the article and approved the submitted version.

DECLARATION OF INTERESTS

The authors declare no competing interests.

Received: August 5, 2023
Revised: February 24, 2024
Accepted: May 1, 2024
Published: May 4, 2024

REFERENCES

1. Gerbaud, P., and Pidoux, G. (2015). Review: An overview of molecular events occurring in human trophoblast fusion. Placenta *36*, S35–S42. https://doi.org/10.1016/j.placenta.2014.12.015.
2. Zeldovich, V.B., Clausen, C.H., Bradford, E., Fletcher, D.A., Maltepe, E., Robbins, J.R., and Bakardjiev, A.I. (2013). Placental syncytium forms a biophysical barrier against pathogen invasion. PLoS Pathog. *9*, e1003821. https://doi.org/10.1371/journal.ppat.1003821.
3. Knöfler, M., Haider, S., Saleh, L., Pollheimer, J., Gamage, T.K.J.B., and James, J. (2019). Human placenta and trophoblast development: key molecular mechanisms and model systems. Cell. Mol. Life Sci. *76*, 3479–3496. https://doi.org/10.1007/s00018-019-03104-6.
4. Hod, M., Kapur, A., Sacks, D.A., Hadar, E., Agarwal, M., Di Renzo, G.C., Cabero Roura, L., McIntyre, H.D., Morris, J.L., and Divakar, H. (2015). The International Federation of Gynecology and Obstetrics (FIGO) Initiative on gestational diabetes mellitus: A pragmatic guide for diagnosis, management, and care. Int. J. Gynaecol. Obstet. *131*, S173–S211. https://doi.org/10.1016/s0020-7292(15)30033-3.
5. Wei, Y., Xu, Q., Yang, H., Yang, Y., Wang, L., Chen, H., Anderson, C., Liu, X., Song, G., Li, Q., et al. (2019). Preconception diabetes mellitus and adverse pregnancy outcomes in over 6.4 million women: A population-based cohort study in China. PLoS Med. *16*, e1002926. https://doi.org/10.1371/journal.pmed.1002926.
6. Kapur, A., McIntyre, H.D., and Hod, M. (2019). Type 2 Diabetes in Pregnancy. Endocrinol. Metab. Clin. North Am. *48*, 511–531. https://doi.org/10.1016/j.ecl.2019.05.009.
7. Nteeba, J., Varberg, K.M., Scott, R.L., Simon, M.E., Iqbal, K., and Soares, M.J. (2020). Poorly controlled diabetes mellitus alters placental structure, efficiency, and plasticity. BMJ Open Diabetes Res. Care *8*, e001243. https://doi.org/10.1136/bmjdrc-2020-001243.
8. Aires, M.B., and Dos Santos, A.C.V. (2015). Effects of maternal diabetes on trophoblast cells. World J. Diabetes *6*, 338–344. https://doi.org/10.4239/wjd.v6.i2.338.
9. Soygur, B., Sati, L., and Demir, R. (2016). Altered expression of human endogenous retroviruses syncytin-1, syncytin-2 and their receptors in human normal and gestational diabetic placenta. Histol. Histopathol. *31*, 1037–1047. https://doi.org/10.14670/HH-11-735.
10. Jones, J.D., Monroe, J., and Koutmou, K.S. (2020). A molecular-level perspective on the frequency, distribution, and consequences of messenger RNA modifications. Wiley Interdiscip. Rev. RNA *11*, e1586. https://doi.org/10.1002/wrna.1586.
11. Zaccara, S., Ries, R.J., and Jaffrey, S.R. (2019). Reading, writing and erasing mRNA methylation. Nat. Rev. Mol. Cell Biol. *20*, 608–624. https://doi.org/10.1038/s41580-019-0168-5.
12. Jiang, X., Liu, B., Nie, Z., Duan, L., Xiong, Q., Jin, Z., Yang, C., and Chen, Y. (2021). The role of m6A modification in the biological functions and diseases. Signal Transduct. Target. Ther. *6*, 74. https://doi.org/10.1038/s41392-020-00450-x.
13. Gu, Y., Chu, X., Morgan, J.A., Lewis, D.F., and Wang, Y. (2021). Upregulation of METTL3 expression and m6A RNA methylation in placental trophoblasts in preeclampsia. Placenta *103*, 43–49. https://doi.org/10.1016/j.placenta.2020.10.016.
14. Wang, J., Gao, F., Zhao, X., Cai, Y., and Jin, H. (2020). Integrated analysis of the transcriptome-wide m6A methylome in preeclampsia and healthy control placentas. PeerJ *8*, e9880. https://doi.org/10.7717/peerj.9880.
15. Qiu, W., Zhou, Y., Wu, H., Lv, X., Yang, L., Ren, Z., Tian, H., Yu, Q., Li, J., Lin, W., et al. (2021). RNA Demethylase FTO Mediated RNA mA Modification Is Involved in Maintaining Maternal-Fetal Interface in Spontaneous Abortion. Front. Cell Dev. Biol. *9*, 617172. https://doi.org/10.3389/fcell.2021.617172.
16. Xu, Z., Tian, P., Guo, J., Mi, C., Liang, T., Xie, J., Huang, W., Dai, M., Chen, W., and Zhang, H. (2021). Lnc-HZ01 with m6A RNA methylation inhibits human trophoblast cell proliferation and induces miscarriage by up-regulating BPDE-activated lnc-HZ01/MXD1 positive feedback loop. Sci. Total Environ. *776*, 145950. https://doi.org/10.1016/j.scitotenv.2021.145950.
17. Wang, J., Wang, K., Liu, W., Cai, Y., and Jin, H. (2021). m6A mRNA methylation regulates the development of gestational diabetes mellitus in Han Chinese women. Genomics *113*, 1048–1056. https://doi.org/10.1016/j.ygeno.2021.02.016.
18. Song, T., Lu, J., Deng, Z., Xu, T., Yang, Y., Wei, H., Li, S., Jiang, S., and Peng, J. (2018). Maternal obesity aggravates the abnormality of porcine placenta by increasing N-methyladenosine. Int. J. Obes. *42*, 1812–1820. https://doi.org/10.1038/s41366-018-0113-2.
19. Shen, W.-B., Ni, J., Yao, R., Goetzinger, K.R., Harman, C., Reece, E.A., Wang, B., and Yang, P. (2022). Maternal obesity increases DNA methylation and decreases RNA methylation in the human placenta. Reprod. Toxicol. *107*, 90–96. https://doi.org/10.1016/j.reprotox.2021.12.002.
20. Yang, Y., Shen, F., Huang, W., Qin, S., Huang, J.-T., Sergi, C., Yuan, B.-F., and Liu, S.-M. (2019). Glucose Is Involved in the Dynamic Regulation of m6A in Patients With Type 2 Diabetes. J. Clin. Endocrinol. Metab. *104*, 665–673. https://doi.org/10.1210/jc.2018-00619.
21. Msheik, H., El Hayek, S., Bari, M.F., Azar, J., Abou-Kheir, W., Kobeissy, F., Vatish, M., and Daoud, G. (2019). Transcriptomic profiling of trophoblast fusion using BeWo and JEG-3 cell lines. Mol. Hum. Reprod. *25*, 811–824. https://doi.org/10.1093/molehr/gaz061.
22. Li, Z.-H., Li, X., Li, F.-F., Wu, Z.-H., Xie, Y.-L., Zhang, S., Chen, X.-M., Wang, Y.-X., Ding, Y.-B., and Liu, T.-H. (2022). The roles of ADAMDEC1 in trophoblast differentiation during normal pregnancy and preeclampsia. Mol. Hum. Reprod. *28*, gaac014. https://doi.org/10.1093/molehr/gaac014.
23. Choi, M., Byun, N., Hwang, J.R., Choi, Y.-S., Sung, J.-H., Choi, S.-J., Kim, J.-S., Oh, S.-Y., and Roh, C.-R. (2022). Effect of hydroxychloroquine and chloroquine on syncytial differentiation and autophagy in primary human trophoblasts. Biomed. Pharmacother. *149*, 112916. https://doi.org/10.1016/j.biopha.2022.112916.
24. Liu, J., Shao, X., Qin, W., Zhang, Y., Dang, F., Yang, Q., Yu, X., Li, Y.-X., Chen, X., Wang, C., and Wang, Y.-L. (2021). Quantitative chemoproteomics reveals O-GlcNAcylation of cystathionine γ-lyase (CSE) represses trophoblast syncytialization. Cell Chem. Biol. *28*, 788–801.e5. https://doi.org/10.1016/j.chembiol.2021.01.024.
25. Gupta, S.K., Malhotra, S.S., Malik, A., Verma, S., and Chaudhary, P. (2016). Cell Signaling Pathways Involved During Invasion and Syncytialization of Trophoblast Cells. Am. J. Reprod. Immunol. *75*, 361–371. https://doi.org/10.1111/aji.12436.
26. Renaud, S.J., Chakraborty, D., Mason, C.W., Rumi, M.A.K., Vivian, J.L., and Soares, M.J. (2015). OVO-like 1 regulates progenitor cell fate in human trophoblast development. Proc. Natl. Acad. Sci. USA *112*, E6175–E6184. https://doi.org/10.1073/pnas.1507397112.
27. Adu-Gyamfi, E.A., Lamptey, J., Chen, X.-M., Li, F.-F., Li, C., Ruan, L.-L., Yang, X.-N., Liu, T.-H., Wang, Y.-X., and Ding, Y.-B. (2021). Iodothyronine deiodinase 2 (DiO) regulates trophoblast cell line cycle, invasion and apoptosis; and its downregulation is associated with early recurrent miscarriage. Placenta *111*, 54–68. https://doi.org/10.1016/j.placenta.2021.06.004.
28. Tian, F.-Y., Wang, X.-M., Xie, C., Zhao, B., Niu, Z., Fan, L., Hivert, M.-F., and Chen, W.-Q. (2018). Placental surface area mediates the association between methylation in placenta and full-term low birth weight in girls. Clin. Epigenetics *10*, 39. https://doi.org/10.1186/s13148-018-0472-5.
29. Li, G., Wang, Y., Cao, G., Ma, Y., Li, Y.-X., Zhao, Y., Shao, X., and Wang, Y.-L. (2022). Hypoxic stress disrupts HGF/Met signaling in human trophoblasts: implications for the pathogenesis of preeclampsia. J. Biomed. Sci. *29*, 8. https://doi.org/10.1186/s12929-022-00791-5.
30. Ning, J., Huai, J., Wang, S., Yan, J., Su, R., Zhang, M., Liu, M., and Yang, H. (2023). METTL3 regulates glucose transporter expression in placenta exposed to hyperglycemia through the mTOR signaling pathway. Chin. Med. J. https://doi.org/10.1097/CM9.0000000000002840.
31. Azar, C., Valentine, M., Trausch-Azar, J., Druley, T., Nelson, D.M., and Schwartz, A.L. (2018). RNA-Seq identifies genes whose proteins are transformative in the differentiation of cytotrophoblast to syncytiotrophoblast, in human primary villous and BeWo trophoblasts. Sci. Rep. *8*, 5142. https://doi.org/10.1038/s41598-018-23379-2.
32. Karahoda, R., Zaugg, J., Fuenzalida, B., Kallol, S., Moser-Haessig, R., Staud, F., and Albrecht, C. (2022). Trophoblast Differentiation Affects Crucial Nutritive Functions of Placental Membrane Transporters. Front. Cell Dev. Biol. *10*, 820286. https://doi.org/10.3389/fcell.2022.820286.
33. Wang, Y.-N., Ye, Y.-X., Guo, Z.-W., Xiong, Z.-L., Sun, Q.-S., Zhou, D., Jiang, S.-W., and Chen, H. (2022). Inducible knockout of syncytin-a leads to poor placental glucose transport in mice. Placenta *121*, 155–163. https://doi.org/10.1016/j.placenta.2022.03.016.
34. Kuc, S., Wortelboer, E.J., Koster, M.P.H., de Valk, H.W., Schielen, P.C.J.I., and Visser, G.H.A. (2011). Prediction of macrosomia at birth in type-1 and 2 diabetic pregnancies with biomarkers of early placentation. BJOG An Int. J. Obstet. Gynaecol. *118*, 748–754. https://doi.org/10.1111/j.1471-0528.2011.02904.x.

35. Raffel, G.D., Chu, G.C., Jesneck, J.L., Cullen, D.E., Bronson, R.T., Bernard, O.A., and Gilliland, D.G. (2009). Ott1 (Rbm15) is essential for placental vascular branching morphogenesis and embryonic development of the heart and spleen. Mol. Cell Biol. *29*, 333–341. https://doi.org/10.1128/MCB.00370-08.
36. Zhou, W., Xue, P., Yang, Y., Xia, L., and Yu, B. (2022). Research progress on N6-methyladenosine in the human placenta. J. Perinat. Med. *50*, 1115–1123. https://doi.org/10.1515/jpm-2021-0665.
37. Darling, N.J., and Cohen, P. (2021). Nuts and bolts of the salt-inducible kinases (SIKs). Biochem. J. *478*, 1377–1397. https://doi.org/10.1042/BCJ20200502.
38. Sakamoto, K., Bultot, L., and Göransson, O. (2018). The Salt-Inducible Kinases: Emerging Metabolic Regulators. Trends Endocrinol. Metab. *29*, 827–840. https://doi.org/10.1016/j.tem.2018.09.007.
39. Fu, Y., Dominissini, D., Rechavi, G., and He, C. (2014). Gene expression regulation mediated through reversible m^{6}A RNA methylation. Nat. Rev. Genet. *15*, 293–306. https://doi.org/10.1038/nrg3724.
40. Bassols, J., Prats-Puig, A., Vázquez-Ruíz, M., García-González, M.M., Martínez-Pascual, M., Avellí, P., Martínez-Martínez, R., Fàbrega, R., Colomer-Virosta, C., Soriano-Rodríguez, P., et al. (2010). Placental FTO expression relates to fetal growth. Int. J. Obes. *34*, 1365–1370. https://doi.org/10.1038/ijo.2010.62.
41. Mayeur, S., Cisse, O., Gabory, A., Barbaux, S., Vaiman, D., Vambergue, A., Fajardy, I., Deloof, S., Junien, C., Laborie, C., et al. (2013). Placental expression of the obesity-associated gene FTO is reduced by fetal growth restriction but not by macrosomia in rats and humans. J. Dev. Orig. Health Dis. *4*, 134–138. https://doi.org/10.1017/S2040174412000748.
42. Liu, Z.-W., Zhang, J.-T., Cai, Q.-Y., Zhang, H.-X., Wang, Y.-H., Yan, H.-T., Wu, H.-M., and Yang, X.-J. (2016). Birth weight is associated with placental fat mass- and obesity-associated gene expression and promoter methylation in a Chinese population. J Matern Fetal Neona *29*, 106–111. https://doi.org/10.3109/14767058.2014.987749.
43. Gulati, P., Cheung, M.K., Antrobus, R., Church, C.D., Harding, H.P., Tung, Y.-C.L., Rimmington, D., Ma, M., Ron, D., Lehner, P.J., et al. (2013). Role for the obesity-related FTO gene in the cellular sensing of amino acids. Proc. Natl. Acad. Sci. USA *110*, 2557–2562. https://doi.org/10.1073/pnas.1222796110.
44. Okae, H., Toh, H., Sato, T., Hiura, H., Takahashi, S., Shirane, K., Kabayama, Y., Suyama, M., Sasaki, H., and Arima, T. (2018). Derivation of Human Trophoblast Stem Cells. Cell Stem Cell *22*, 50–63.e6. https://doi.org/10.1016/j.stem.2017.11.004.
45. Li, X., Li, Z.-H., Wang, Y.-X., and Liu, T.-H. (2023). A comprehensive review of human trophoblast fusion models: recent developments and challenges. Cell Death Discov. *9*, 372. https://doi.org/10.1038/s41420-023-01670-0.
46. Martin, M. (2011). Martin M.Cut adapt removes adapter sequences from high-throughput sequencing reads. EMBnet. j. *17*, 10–12.
47. Kim, D., Langmead, B., and Salzberg, S.L. (2015). HISAT: A fast spliced aligner with low memory requirements. Nat. Methods *12*, 357–360.
48. Zhang, Y., Liu, T., Meyer, C.A., Eeckhoute, J., Johnson, D.S., Bernstein, B.E., Nusbaum, C., Myers, R.M., Brown, M., Li, W., and Liu, X.S. (2008). Model-based analysis of ChIP-Seq (MACS). Genome Biol. *9*, R137. https://doi.org/10.1186/gb-2008-9-9-r137.
49. Shen, L., Shao, N.-Y., Liu, X., Maze, I., Feng, J., and Nestler, E.J. (2013). diffReps: detecting differential chromatin modification sites from ChIP-seq data with biological replicates. PLoS One *8*, e65598. https://doi.org/10.1371/journal.pone.0065598.
50. Orendi, K., Gauster, M., Moser, G., Meiri, H., and Huppertz, B. (2010). The choriocarcinoma cell line BeWo: syncytial fusion and expression of syncytium-specific proteins. Reproduction (Cambridge, England) *140*, 759–766. https://doi.org/10.1530/REP-10-0221.
51. Meyer, K.D., Saletore, Y., Zumbo, P., Elemento, O., Mason, C.E., and Jaffrey, S.R. (2012). Comprehensive analysis of mRNA methylation reveals enrichment in 3' UTRs and near stop codons. Cell *149*, 1635–1646. https://doi.org/10.1016/j.cell.2012.05.003.
52. Matsukawa, H., Ikezaki, M., Nishioka, K., Iwahashi, N., Fujimoto, M., Nishitsuji, K., Ihara, Y., and Ino, K. (2022). Calnexin Is Involved in Forskolin-Induced Syncytialization in Cytotrophoblast Model BeWo Cells. Biomolecules *12*, 1050. https://doi.org/10.3390/biom12081050.

STAR★METHODS

KEY RESOURCES TABLE

REAGENT or RESOURCE	SOURCE	IDENTIFIER
Antibodies		
Rabbit monoclonal anti-β-actin (13E5)	Cell Signaling Technology	Cat#: 4970; RRID: AB_10694076
Rabbit polyclonal anti-FTO	Proteintech	Cat#: 27226-1-AP; RRID: AB_2880809
Rabbit polyclonal anti-SIK1	Proteintech	Cat#: 51045-1-AP; RRID: AB_2187322
Rabbit polyclonal anti-β-hCG	Proteintech	Cat#: 11615-1-AP; RRID: AB_2877783
Rabbit Polyclonal anti-SYNC-2 (N-term)	Abcepta	Cat#: AP13018A; RRID: AB_10821694
Anti-Rabbit IgG-HRP	Cell Signaling Technology	Cat#: 7074; RRID: AB_2099233
Rabbit monoclonal anti-E-cadherin	Cell Signaling Technology	Cat#: 3195; RRID: AB_2291471
Goat Anti-Rabbit IgG H&L (Alexa Fluor 488)	Abcam	Cat#: ab150077; RRID: AB_2630356
Chemicals, peptides, and recombinant proteins		
Forskolin (FSK)	Selleck	S2449
D-glucose	Sigma-Aldrich	G8270
D-mannitol	Sigma-Aldrich	M1902
Actinomycin D	MedChemExpress	HY-17559
Critical commercial assays		
Dual-Luciferase Reporter Assay System	Promega	E1910
GenSeq m6A RNA IP Kit	GenSeq	GS-ET-00110
NEBNext® Ultra II Directional RNA Library Prep Kit	New England Biolabs	E7530
Deposited data		
Raw and analyzed data	This paper	GSA-Human: HRA004981
Experimental models: Cell lines		
Human choriocarcinoma BeWo cells	NICR	1101HUM-PUMC000156
Oligonucleotides		
Primers for qRT-PCR, see Table S3	This paper	N/A
Primers for MeRIP-qPCR, see Table S4	This paper	N/A
siRNA targeting sequence: FTO: CAGGAACCUUGGAUUAUAUTT	This paper	N/A
siRNA targeting sequence: SIK1: CAGGAACCUUGGAUUAUAUTT	This paper	N/A
siRNA targeting sequence: a noncoding scrambled sequence: UUCUCCGAACGUGUCACGUTT	This paper	N/A
Recombinant DNA		
Plasmid: FTO and negative control	This paper	N/A
WT or MUT SIK1-3′-UTR inserted downstream of firefly luciferase in a GV272 vector	This paper	N/A
Software and algorithms		
ImageJ	NIH	https://imagej.net/NIH_Image
GraphPad Prism 9	Graphpad	https://www.graphpad.com/scientific-software/prism/
SPSS software version 26.0	IBM	https://www.ibm.com/products/spss-statistics
Image-Pro Plus 6.0	Media Cybernetics	https://mediacy.com/image-pro/

(*Continued on next page*)

Continued

REAGENT or RESOURCE	SOURCE	IDENTIFIER
Cutadapt software (v1.9.3)	Martin et al.[46]	N/A
HISAT2 software (v2.0.4)	Kim et al.[47]	N/A
MACS software (1.4.2)	Zhang et al.[48]	N/A
DiffReps software	Shen et al.[49]	N/A

RESOURCE AVAILABILITY

Lead contact

Further information and requests for resources and reagents should be directed to and will be fulfilled by the lead contact, Huixia Yang (yanghuixia@bjmu.edu.cn).

Materials availability

This study did not generate new unique reagents.

Data and code availability

The raw sequence data reported in this paper have been deposited in the Genome Sequence Archive (Genomics, Proteomics & Bioinformatics 2021) in National Genomics Data Center (Nucleic Acids Res 2022), China National Center for Bioinformation/Beijing Institute of Genomics, Chinese Academy of Sciences (GSA-Human: HRA004981), which are publicly accessible at https://ngdc.cncb.ac.cn/gsa-human.

This paper does not report original code.

Any additional information required to reanalyze the data reported in this work paper is available from the lead contact upon request.

EXPERIMENTAL MODEL AND STUDY PARTICIPANT DETAILS

Human participants

Term human placenta samples from Han Chinese women with poorly controlled type 2 diabetes (T2DM, n = 12; age 27–40 years, mean 35.3 years) and normal pregnancies (CTRL, n = 15; age 29–41 years, mean 34.8 years) were obtained from Peking University First Hospital, and individual women gave their informed consent for use of the placenta specimens. The Ethics Committee of Peking University First Hospital approved this study (reference no. 2013-572). Type 2 diabetes was defined using the International Federation of Gynecology and Obstetrics guidelines.[4] In this study, poorly controlled glycemia was defined as hemoglobin A1c (HbA1c) or glycated albumin (GA) levels greater than 6% or 16%, respectively, at least once throughout pregnancy. The clinical characteristics of all study participants are shown in Tables S1 and S2. The villus tissue from the maternal surface of the placenta and full-thickness placental tissue were dissected from a region 5 cm away from the umbilical cord insertion within 0.5 h after cesarean section delivery for subsequent detection.

Cell lines

Human choriocarcinoma BeWo cells (RRID: CVCL_0044), which are used extensively in models of trophoblast differentiation and syncytialization, were purchased from the National Infrastructure of Cell Line Resource (NICR).[45,50] Cells were grown in Roswell Park Memorial Institute (RPMI) 1640 medium (Sigma, St. Louis, MO, USA) containing 10% fetal bovine serum (FBS) (Sigma Aldrich, St. Louis, MO, USA) and 1% antibiotic-antimycotic (Gibco, Grand Island, NY, USA) at 37°C in 5% CO2. This cell line was authenticated with STR profiling and was also checked free of mycoplasma contamination by polymerase chain reaction (PCR) and culture.

To mimic normal and abnormal glycemia states that may be encountered among pregnant women with type 2 diabetes, BeWo cells were cultured in the 25 mM D-glucose (hyperglycemia) (Sigma Aldrich) and 5.5 mM D-glucose + 19.5 mM D-mannitol (osmotic control) (Sigma Aldrich) added to RPMI 1640 with no glucose (ThermoFisher, Scientific, Wilmington, MA, USA). In addition, BeWo cells were treated with FSK (20 μM, Selleck, Houston, Texas, USA) to achieve cell fusion, and BeWo cells treated with dimethyl sulfoxide (DMSO, Sigma Aldrich) served as the control.

METHOD DETAILS

RNA m6A quantification

The m6A RNA methylation status of total RNA was detected using the EpiQuik™ m6A RNA Methylation Quantification Kit (Colorimetric, Epigentek, Farmingdale, NY, USA) according to the manufacturer's instructions. Briefly, 200 ng of total RNA accompanied by a negative control and m6A standard were bound to 96-well plates, followed by diluted capture anti-m6A antibody solution and detection antibody solution. The optical density at 450 nm was measured to quantify the amount of m6A.

RNA extraction and real-time quantitative PCR (RT–qPCR)

We reverse-transcribed total RNA (2 μg) from placental tissue and cells into complementary DNA (cDNA) using FastKing gDNA Dispelling RT SuperMix (Tiangen Biotech, Beijing, China) and we carried out RT–qPCR using SYBR Green Real-Time PCR Master Mix (Bimake, Houston, TX, USA) with β-actin as an internal control. The sequences of primers used in the study are shown in Table S3.

Western blotting (WB)

Cells were harvested and lysed in RIPA (Bioss, Beijing, China) lysis buffer. Approximately 30 μg of protein was separated by 12% sodium dodecyl sulfate -polyacrylamide gel electrophoresis (SDS-PAGE) and then transferred onto PVDF membranes (Millipore, Bedford, MA, USA). Membranes were incubated with the following primary antibodies: FTO (Proteintech, Wuhan, China; 1:1000; RRID: AB_2880809), SIK1 (Proteintech; 1:1000; RRID: AB_2187322), β-hCG (Proteintech; 1:1000; RRID: AB_2877783), SYNC-2 (Abcepta, San Diego, USA; 1:1000; RRID: AB_10821694), and β-actin (Cell Signaling Technology, Danvers, USA; 1:2000; RRID: AB_10694076). After incubation with HRP-conjugated secondary antibodies (Cell Signaling Technology; 1:2000; RRID: AB_2099233) at room temperature (RT) for 90 min, the signals were identified by an enhanced chemiluminescence reagent (Merck Millipore).

Immunohistochemistry

The paraffin-embedded blocks of full-thickness placental tissues were cut into 4 μm-thick sections. After deparaffinization, hydration, antigen retrieval and endogenous peroxidase clearance, the slides were incubated overnight at 4°C in a humidified chamber with rabbit polyclonal antibodies against FTO (Proteintech; 1:2000), SIK1 (Proteintech; 1:500), β-hCG (Proteintech; 1:1000) or SYNC-2 (Abcepta, San Diego, USA; 1:500) followed by incubation with HRP-conjugated secondary antibody. We detected signals using a diaminobenzidine kit (ZSGB-BIO, Beijing, China) and analyzed the digital images using Image-Pro Plus 6.0. The average optical density (integrated optical density [IOD]/area) of each image was used to reflect protein expression.

MeRIP-seq and data analysis

MeRIP-Seq was performed by Cloudseq Biotech Inc. (Shanghai, China) according to the published procedure[51] with slight modifications. Briefly, m6A RNA immunoprecipitation was performed with the GenSeqTM m6A RNA IP Kit (GenSeq Inc., China) following the manufacturer's instructions. Both the input sample (without immunoprecipitation) and the m6A IP samples were used for RNA-seq library generation with the NEBNext® Ultra II Directional RNA Library Prep Kit (New England Biolabs, Inc., USA). The library quality was evaluated with a BioAnalyzer 2100 system (Agilent Technologies, Inc., USA). Library sequencing was performed on an Illumina NovaSeq instrument with 150 bp paired-end reads.

Paired-end reads were harvested from an Illumina NovaSeq 6000 sequencer and were quality controlled by Q30. After 3′ adaptor trimming and low-quality read removal, cutadapt[46] software (v1.9.3) was used. First, clean reads of all libraries were aligned to the reference genome (UCSC HG19) by HISAT2[47] software (v2.0.4). Methylated sites on RNAs (peaks) were identified by MACS (1.4.2)[48] software with default parameters. And DiffReps[49] software identified differentially methylated genes between T2DM and CTRL placenta (n=5) with the criteria of a P value $\leq$ 0.00001 and a fold change $\geq$2 or < 0.5. The peaks that overlap with exon regions were screened using bedtools intersect and annotated accordingly. Gene Ontology (GO) and pathway enrichment analyses were performed using the differentially-methylated protein-coding genes.

RNA sequencing

RNA sequencing was performed by Cloudseq Biotech Inc. according to the manufacturer's protocol. The constructed sequencing library was quality-controlled and quantified by the BioAnalyzer 2100 system (Agilent Technologies), and then library sequencing was performed on an Illumina NovaSeq instrument with 150 bp paired-end reads. The significantly differentially expressed genes between the two groups were identified with the criteria of a P value $\leq$ 0.05 and a fold change $\geq$2 or < 0.5.

Gene-specific m6A qPCR (MeRIP-qPCR)

Total RNA from the placentas of the two groups was fragmented to approximately 100 nt in length, and the fragmented RNA was incubated with m6A antibody-coated beads. Methylated RNAs bound to magnetic beads were eluted and purified. The m6A modification of target genes was verified by qPCR, and the primers used for detection of m6A-enriched gene mRNA are listed in Table S4.

Cell transfection

BeWo cells were transfected with small interfering RNAs (siRNAs) (GenePharma, Suzhou, China) targeting FTO (100 nM; 5′ CAGGAA CCUUGGAUUAUAUTT 3′), SIK1 (100 nM; 5′ GGAACCAGCUCUGACAGUUTT 3′), or a noncoding scrambled sequence (100 nM; 5′ UUCUCCGAACGUGUCACGUTT 3′) using Lipofectamine RNA iMax (Invitrogen, Carlsbad, CA, USA) according to the manufacturer's protocol. For FTO overexpression (OE) experiments, BeWo cells were transfected with FTO-DN and pc-DNA (as the negative control) plasmids by using Lipofectamine 3000 (Invitrogen, Carlsbad, CA, USA) following the manufacturer's instructions.

mRNA stability

BeWo cells were treated with actinomycin D (5 μg/mL; MedChemExpress) in medium with different treatments and collected at 0, 6, and 12 h. Then, the total RNA was extracted for qPCR as described above. The mRNA expression for each group at the indicated time was calculated and the data were normalized to β-actin.

Immunofluorescence and image analysis

The cells were fixed onto slides with 4% formaldehyde for 10 min and then permeabilized with Saponin/Triton X-100 (Beyotime Biotechnology, Shanghai, China) for 10 min. The cells were stained with diluted primary antibodies against E-cadherin (Cell Signaling Technology; 1:400; RRID: AB_2291471) for 12-18 h at 4°C and diluted Alexa Fluor 488-labeled rabbit secondary antibody (Abcam; 1:1000; RRID: AB_2630356) for 1 h at RT. Then, the cells were stained with DAPI, and the slides were sealed with coverslips. Confocal laser scanning microscopy was performed using a Leica SP8 confocal microscope and images were recorded with a 63× oil immersion objective. To quantify cell fusion, we counted both the total number of nuclei and the number of nuclei in multinucleated cells (containing two or more nuclei) and the percentages of fused cells (fusion index) were calculated as the ratio of the number of nuclei within multinucleated cells to the total nuclei.[52]

Dual-luciferase reporter assays

The DNA fragments of the SIK1-3′-untranslated regions (UTRs) containing the wild-type m6A motifs, as well as mutant motifs (m6A was replaced by T), were directly synthesized by GeneChem (Shanghai, China). Wild-type (WT) SIK1 and mutant (MUT) SIK1-3′-UTR were inserted downstream of firefly luciferase in a GV272 vector. For the dual-luciferase reporter assay, WT or MUT SIK1-3′-UTR and FTO-DN or pc-DN (CTRL) plasmids were cotransfected into BeWo cells in 6-well plates. The relative luciferase activities were assessed 48 h after transfection by the Dual-Luciferase Reporter Assay System (Promega, Madison, USA). Each group was repeated in triplicate.

SIK1-3′-UTR with wild-type m6A sites

GGCTGCTCCCAGGCCCCCCAGCCGGCCCCTGCCCCGTTTGTGATCGCCCCCTGTGATGGCCCTGGGGCTGCCCCGCTCCCCAGCAC
CCTCCTCACGTCGGGGCTCCCGCTGCTGCCGCCCCCACTCCTGCAGACCGGCGCGTCCCCGGTGGCCTCAGCGGCGCAGCTCCT
GGACACACACCTGCACATTGGCACCGGCCCCACCGCCCTCCCCGCTGTGCCCCCACCACGCCTGGCCAGGCTGGCCCCAGGTTGTG
AGCCCCTGGGGCTGCTGCAGGG**GGACT**GTGAGATGGA**GGACC**TGATGCCCTGCTCCCTAGGCACGTTTGTCCTGGTGCAGTGAGGG
CAGCCCTGCATCCTGGCAC**GGACA**C**TGACT**CTTACAGCAATAACTTCAGAGGAGGTGAAGACATCTGGCCTCAAAGCCAA**GAACT**TTC
TAGAAGCGAAATAAGCAATACGTTAGGTGTTTTGGCTTTTTAGTTTATTTTTGTTTTATTTTTTTCTTGCACTGAGTGACCTCAACTTTGAGT
AG**GGACT**GG**AAACT**TTAGGAAGAAAGATAATTGAGGG.

SIK1-3′-UTR with mutated m6A sites

GGCTGCTCCCAGGCCCCCCAGCCGGCCCCTGCCCCGTTTGTGATCGCCCCCTGTGATGGCCCTGGGGCTGCCCCGCTCCCCAGCAC
CCTCCTCACGTCGGGGCTCCCGCTGCTGCCGCCCCCACTCCTGCAGACCGGCGCGTCCCCGGTGGCCTCAGCGGCGCAGCTCCT
GGTCACACACCTGCACATTGGCACCGGCCCCACCGCCCTCCCCGCTGTGCCCCCACCACGCCTGGCCAGGCTGGCCCCAGGTTGTG
AGCCCCTGGGGCTGCTGCAGGG**GGTCT**GTGAGATGGA**GGTCC**TGATGCCCTGCTCCCTAGGCACGTTTGTCCTGGTGCAGTGAGGG
CAGCCCTGCATCCTGGCAC**GGTCA**C**TGTCT**CTTACAGCAATAACTTCAGAGGAGGTGAAGACATCTGGCCTCAAAGCCAA**GATCT**TTC
TAGAAGCGAAATAAGCAATACGTTAGGTGTTTTGGCTTTTTAGTTTATTTTTGTTTTATTTTTTTCTTGCACTGAGTGACCTCAACTTTGAGT
AG**GGTCT**GG**AATCT**TTAGGAAGAAAGATAATTGAGGG.

QUANTIFICATION AND STATISTICAL ANALYSIS

Statistical analysis was performed using SPSS software version 26.0 and the quantitative data are shown as the mean ± standard deviation (SD). The data was evaluated using an unpaired Student's *t* tests (for parametric data) or the Mann–Whitney test (for nonparametric data) when analyzing two groups. When three or more groups were compared, one-way ANOVA with least—significant difference (LSD) was used for parametric data and Friedman's tests was used for nonparametric data. Significance was defined as $^{*}p < 0.05$, $^{**}p < 0.01$, $^{***}p < 0.001$, $^{****}p < 0.0001$.